PHYSICAL REVIEW B **81**, 100506(R) (2010)

Shear banding and spatiotemporal oscillations in vortex matter in nanostructured superconductors

C. Reichhardt and C. J. Olson Reichhardt
Theoretical Division, Los Alamos National Laboratory, Los Alamos, New Mexico 87545, USA
(Received 16 December 2009; published 10 March 2010)

We propose a simple nanostructured pinning array geometry where a rich variety of complex vortex shear banding phenomena can be realized. A single row of pinning sites is removed from a square pinning array. Shear banding effects arise when vortex motion in the pin-free channel nucleates motion of vortices in the surrounding pinned regions, creating discrete steps in the vortex velocity profile away from the channel. Near the global depinning transition, the width of the band of moving vortices undergoes oscillations or fluctuations that can span the entire system. We use simulations to show that these effects should be observable in the transport properties of the system. Similar large oscillations and shear banding effects are known to occur for sheared complex fluids in which different dynamical phases coexist.

DOI: 10.1103/PhysRevB.81.100506 PACS number(s): 74.25.Uv, 74.25.Wx

Sheared complex fluids[1–6] and colloidal assemblies[7] exhibit the dynamical phenomenon of *shear banding* (SB), in which the motion of the system under an applied shear becomes stratified or concentrated in certain regions. For many complex fluids where different dynamical flow phases can coexist, coupling of these phases under shear can induce additional dynamics such as large oscillations and strongly fluctuating chaotic phases.[5,6] It would be interesting to explore whether similar behaviors can occur in other systems such as magnetic vortices in type-II superconductors. Shear banding induced by the presence of periodic structures, such as a periodic pinning array for superconducting vortices, has not been considered previously. Shearing in complex fluids or colloids in the presence of quenched disorder could be realized by having the flow traverse an optical trap array or a periodic array of micron-scale obstacles.

In order to shear a superconducting vortex system, unconventional contact geometries such as the Corbino geometry are normally used.[8–12] Simulations of pin-free systems using such geometries show transitions from rigid body rotation to liquidlike flow states,[13] and experiments revealed a similar effect near the vortex liquid to vortex solid transition.[8] In other experiments, noise and transport measurements of moving vortices were performed in a Corbino geometry.[9,12] Recent simulations of Corbino contacts applied to very small superconducting disks produced a wide variety of vortex dynamics.[14] In this work we propose the use of a simple periodic pinning array geometry rather than a Corbino geometry to shear the vortices. We observe a rich variety of shear banding effects including an ordered phase with velocity steps, giant spatiotemporal oscillations, and strongly fluctuating chaotic phases.

Using nanotechnology it is now possible to create tailored pinning array structures in which the lattice symmetry and the order and size of the pinning sites can be carefully controlled.[15,16] It has also been demonstrated experimentally that these arrays can be diluted by systematically removing individual pinning sites.[17] Here we propose removing entire rows from a square pinning array and applying a magnetic field such that the vortex density matches the density of the original undiluted square pinning array. Experimentally, this geometry could also be achieved on a larger scale by periodically removing rows of pinning sites. We consider samples in which the pinning sites are sufficiently small that each pin can capture only a single vortex; thus, when there are more vortices than pinning sites, a portion of the vortices are located outside the pinning sites in the pin-free regions. Although this geometry is relatively simple, it has not been considered in previous simulations or experiments. Simulations of vortex dynamics in square pinning arrays near and just above the first matching field showed that the interstitial vortices are more mobile than the pinned vortices and depin at lower driving currents, while coupling between the moving interstitial vortices and the pinned vortices can produce a series of transitions between different dynamical phases including a disordered or turbulent phase with a crossover to a laminar phase at higher drives.[18] Although the simulations provided clear predictions for features in the transport curves associated with these transitions, the experimental observation of these phases was not achieved until very recently due to new experimental capabilities for reducing local heating effects[19] and for performing transport measurements at temperatures well below T_c.[20] Molecular-dynamics-style simulations should serve as excellent models for the experiments that are currently possible.

In this work we demonstrate that when a row or rows of pinning sites are removed from a square pinning array, the vortex motion under an applied driving current first occurs in the pin-free channel and nucleates the depinning and motion of the vortices in the pinning sites. This produces a series of steps in the velocity response along with fluctuating or chaotic phases and giant temporal oscillations when a band of moving vortices propagates away from and toward the pin-free channel.

We simulate a two-dimensional system of superconducting vortices interacting with a modified square pinning array. The sample is of size $L \times L$ and has periodic boundary conditions in the x and y directions. The undiluted square pinning array contains $N_p=361$ pinning sites at a density of $n_p=N_p/L^2$, and the sample contains N_v vortices at a density of $n_v=N_v/L^2$. We take $L=36\lambda$, where λ is the London penetration depth. The field at which $N_v=N_p$ is the matching field B_ϕ. The dynamics of a vortex i at position $\mathbf{R}_i$ is given by the overdamped equation of motion

$$\eta\frac{d\mathbf{R}_i}{dt} = \mathbf{F}_i^{vv} + \mathbf{F}_i^{p} + \mathbf{F}^{ext}. \quad (1)$$

The damping constant $\eta = \phi_0^2 d/2\pi\epsilon^2\rho_N$ in a crystal of thickness d, where $\phi_0 = h/2e$ is the flux quantum, η is the superconducting coherence length, and ρ_N is the normal-state resistivity of the material. The repulsive vortex-vortex interaction force is $\mathbf{F}_i^{vv} = \Sigma_{i\neq j}^{N_v} F_0 K_1(R_{ij}/\lambda)\hat{\mathbf{R}}_{ij}$. Here K_1 is a modified Bessel function that decays exponentially at large distances, $F_0 = \phi_0/2\pi\mu_0\lambda^3$, μ_0 is the permeability of free space, $R_{ij} = |\mathbf{R}_i - \mathbf{R}_j|$, and $\hat{\mathbf{R}}_{ij} = (\mathbf{R}_i - \mathbf{R}_j)/R_{ij}$. The vortex-vortex interaction is cut off at $R_{ij} = 7\lambda$ for efficiency. We have tested the effects of the cutoff carefully in previous simulations and find no changes if the cutoff is modified.[18,21] The pinning sites are modeled as parabolic traps with a maximum force of F_p and radius $R_p = 0.35\lambda$ which are placed in a square array with lattice constant $a = 1.89\lambda$: $\mathbf{F}_i^p = \Sigma_k^{N_p} F_p F_0(R_{ik}/R_p)\Theta(R_p - R_{ik})\hat{\mathbf{R}}_{ik}$, where Θ is the Heaviside step function. We set $n_p = 0.28/\lambda^2$. We keep R_p and F_p small enough that a maximum of one vortex can be captured by a given pinning site, and we remove one row of pins. The initial vortex positions are obtained through simulated annealing, which produces a square vortex arrangement at the matching field $B = B_\phi$. The external driving force $\mathbf{F}^{ext} = F_D\hat{\mathbf{x}}$ represents the Lorentz force from an applied current. We increase F_D in small increments and measure the vortex velocity averaged over $\tau = 8000$ simulation time steps, $\langle V_x\rangle = N_v^{-1}\tau^{-1}\Sigma_t^{\tau}\Sigma_i^{N_v} d\mathbf{R}_i(t)/dt\cdot\hat{\mathbf{x}}$.

In Fig. 1(a) we plot the velocity $\langle V_x\rangle$ versus force F_D/F_p curve for a sample with $F_p = 0.1$ and $B/B_\phi = 1.0$. The central portion of the sample is illustrated in Fig. 1(b) at $F_D/F_p = 0.6$, where only the interstitial vortices in the pin-free row are in motion. There are four distinct regimes in Fig. 1(a). In the pinned regime at low F_D, the interstitial vortices in the pin-free channel remain pinned due to the repulsive interactions from the vortices at the pinning sites. At higher drives, the interstitial vortices depin and enter the single channel flow (SCF) state illustrated in Fig. 1(b). A sharp increase in $\langle V_x\rangle$ occurs near $F_D/F_p = 0.75$ and corresponds to the onset of motion of the vortices in pinning rows adjacent to the pin-free channel, termed the SB regime. The velocity of the vortices moving along the pinning rows is less than the velocity of the vortices in the pin-free channel, and during the time interval required for the vortices in the pinning rows to move a distance a and hop from one pinning site to another, the vortices in the pin-free channel move a distance $2a$ or greater. A small step in $\langle V_x\rangle$ appears when the motion of the vortices in the adjacent pinning sites locks into step with the motion of the vortices in the pin-free channel. For $F_D/F_p > 0.855$ all the vortices are mobile and $\langle V_x\rangle$ increases linearly with increasing F_D/F_p. For $0.83 \leq F_D/F_p \leq 0.855$, $\langle V_x\rangle$ takes a value that is close to half of the Ohmic value, indicating that on average half of the vortices in the sample are moving. It is not clear from the time-averaged data whether this means that half of the vortices are always moving and the other half are always pinned or whether the number of moving vortices is fluctuating. To clarify this, in the inset of Fig. 1(a) we plot $\langle V_x\rangle$ over a small range of F_D/F_p using a shorter time average of $\tau = 175$ simulation time steps. For $0.83 < F_D/F_p < 0.85$, this $\langle V_x\rangle$ response exhibits large oscillations with a maximum velocity close to the Ohmic value and a minimum velocity close to that associated with vortices flowing in three rows, indicating that the number of moving vortices is oscillating over time. In Fig. 1(c) we plot the instantaneous V_x versus time at fixed $F_D/F_p = 0.7$, 0.85, and 0.92. For $F_D/F_p = 0.7$, only three vortex rows are moving and there is a high-frequency periodic component of V_x produced by the motion of the vortices over the periodic pinning sites. For $F_D/F_p = 0.92$, all of the vortices are moving and there is again a high-frequency periodic signal in V_x caused by the periodic motion over the pinning sites. At $F_D/F_p = 0.85$, pronounced oscillations appear in V_x that have a much larger amplitude and a lower frequency, indicating that these oscillations are not associated with the periodicity of the pinning sites. A high-frequency oscillatory component of V_x which is a result of the motion over the periodic pinning sites does appear; however, the larger scale oscillations are due to the emission and absorption of a transverse front of moving vortices originating at the pin-free channel.

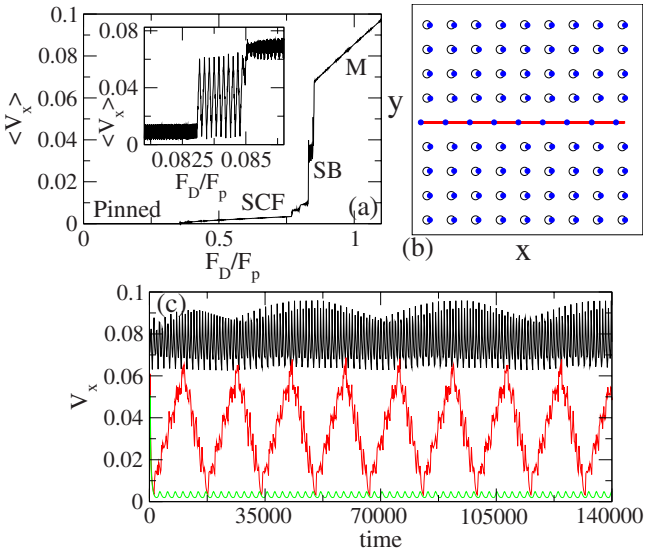

FIG. 1. (Color online) (a) The average velocity $\langle V_x\rangle$ vs applied force F_D/F_p for a system with $F_p = 0.1$, $B/B_\phi = 1.0$, and a single removed row of pinning. Four regimes are marked: a pinned regime, a single channel flow (SCF) regime, a shear banding (SB) regime, and a moving (M) phase in which all of the vortices are flowing. Inset: a blowup of the main panel for $0.081 \leq F_D/F_p \leq 0.0865$ in the shear banding phase where a short time average is used for the velocities so that the fluctuations can be seen more clearly. Large scale oscillations occur as the system switches back and forth between three moving rows of vortices and all rows of vortices moving. On a long time average, the oscillating regime has an intermediate value of $\langle V_x\rangle$ as shown in the main panel. (b) The vortex positions (dots), trajectories (lines), and pinning site locations (open circles) for a small subsection of the sample in (a) in the SCF phase at $F_D/F_p = 0.6$. (c) V_x vs time for the system in (a) at $F_D/F_p = 0.7$, 0.85, and 0.92 (from bottom to top).

In Fig. 2 we illustrate the vortex trajectories during consecutive time intervals for the system shown in Fig. 1(c) at

FIG. 2. (Color online) The vortex positions (dots), trajectories (lines), and pinning site locations (circles) for the system in Fig. 1(c) at $F_D/F_p=0.85$ during consecutive time intervals in a single large oscillation of V_x with period T. (a) At a minimum in V_x, $t/T=0$, the vortices in the pin-free channel move along with vortices in one pinned row on each side of the channel. (b) At $t/T=0.125$, a front of moving rows begins to propagate outwards from the pin-free channel and here three pinned rows on each side of the channel are moving. (c) Near $t/T=0.25$ the moving region continues to grow. (d) At $t/T=0.5$ the front has moved completely through the sample and all of the vortices are moving. (e) Near $t/T=0.8$ the moving region is contracting. (f) At $t/T=1$ the system returns to the minimum state of three moving rows of vortices.

$F_D/F_p=0.85$ for a single cycle of the large oscillations in V_x, which has a period of $T=15\,750$ simulation time steps. At the start of the cycle, V_x is at its minimum value and the vortices in the pin-free channel are moving along with vortices in the two adjacent pinning rows. Figures 2(a)–2(c) shows that during the first half of the oscillation, $t/T<0.5$, an increasing number of vortices in the pinning rows become mobile, and there is a well defined front between the moving and nonmoving portions of the sample. At the halfway point of the oscillation, $t/T=0.5$, Fig. 2(d) indicates that all of the vortices are mobile. When the two depinning fronts meet, an instability is triggered that causes the vortices to become pinned again, and two pinning fronts begin to propagate back toward the pin-free channel during the second half of the

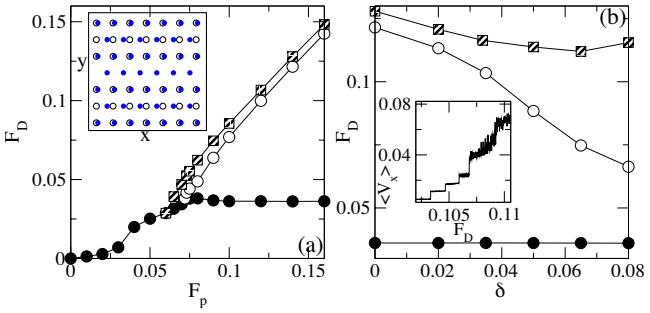

FIG. 3. (Color online) The dynamic phase diagram F_D vs F_p for the system in Fig. 1. Filled circles: depinning transition. Open circles: transition from the SCF to the SB state. Hatched squares: transition from the SB state to the moving state. Inset: Vortex positions (filled circles) and pin positions (open circles) in a small portion of the sample illustrating the depinning process for $F_p<0.6$. Depinning occurs in a single step from a partially pinned elastic solid where half of the vortices are shifted off the pinning sites, as shown. (b) The phase diagram F_D vs δ for the same system with $F_p=0.14$, where δ is a measure of strength dispersion for the pinning sites. As δ increases, the width of the SB region grows. Inset: For $\delta=0.035$, there are more steps in $\langle V_x \rangle$ vs F_D at the onset of the shear banding and the large oscillations are replaced with a fluctuating or chaotic regime.

period, $0.5<t/T<1$. Finally at $t/T=1$, the system returns to the initial state containing only three moving rows of vortices. The period T of the oscillations at fixed F_D depends on the system size since the depinning and pinning fronts propagate at a fixed speed. By simulating large systems, we find that T scales with L. The high-frequency periodic component of the vortex motion that is generated when the vortices move over the periodic pinning array does not change with system size and is a function only of the pinning lattice constant a. Shear banding effects resulting in large oscillations have been observed for shearing in many complex fluids and are due to a nonlinear coupling between two different types of coexisting structures that form in the fluid.[5,6] In our vortex system the two structures are the square pinned vortex lattice and the distorted hexagonal ordering of the moving vortices. The mismatch between these two phases results in the formation of topological defects at the boundary between the phases. When the depinning fronts meet, it is possible that a portion of the defects annihilate, changing the direction of propagation of the front.

In Fig. 3(a) we show a phase diagram of F_D versus F_p highlighting the different phases. For weak pinning, $F_p<0.06$, the depinning transition occurs elastically in a single step where all of the vortices begin moving at the same time. The effect of removing one pinning row is negated by the fact that the vortex ground state for weak pinning forms a distorted triangular lattice by shifting half the vortices off the pinning sites, as shown in the inset of Fig. 3(a). The presence of the pin-free channel merely removes the degeneracy of the ground state and ensures that this shift occurs along the x direction. For $F_p>0.078$, the initial depinning occurs plastically and the vortex motion first occurs in the pin-free channel. The depinning force saturates with increasing F_p since the vortices in the pin-free channel are

pinned by their interactions with the neighboring pinned vortices, and this interaction strength does not depend on F_p. The transition to the moving phase shifts linearly to higher F_D with increasing F_p. Open circles in Fig. 3(a) indicate the transition from the SCF to the SB giant oscillation regime where multiple rows of vortices are moving. For strong pinning, the SB oscillation region is narrow; however, the addition of disorder or an increase in the size of the pinning sites can extend the width of the SB region. To examine the effect of disorder, we changed the pinning strength from uniform to a normal distribution with mean F_p and width δ. In Fig. 3(b), we plot the onset of the different phases for F_D versus δ for a system with $F_p=0.14$. As δ increases, the depinning transition to the SCF regime is unchanged since the depinning force is determined by the fixed vortex-vortex interaction strength. The onset of the SB regime shifts to higher F_D with increasing disorder. For $\delta<0.035$, the dynamics are the same as those illustrated in Fig. 1(a); however, for larger δ the shear banding occurs in a series of steps and the large oscillation region is replaced with a strongly fluctuating or chaotic regime. In the inset of Fig. 3(b) we plot $\langle V_x \rangle$ vs F_D near the onset of the SB regime for $\delta=0.035$. Here there are four steps that correspond to the opening of additional mobile rows of vortices. The steps are followed by a transition to a more strongly fluctuating regime where additional moving rows open and close intermittently.

In summary, we propose a simple periodic pinning geometry for vortices in superconductors in which a rich variety of complex shear banding phenomena can be realized. A single row of pinning sites is removed to create an easy flow channel. Under an applied drive the vortices in the channel move first but due to their coupling with the vortices in the adjacent pinning sites, vortex motion along the neighboring rows is also nucleated. As the global depinning transition is approached, bands of moving rows of vortices propagate away from and toward the channel, creating giant spatiotemporal oscillations which can be seen in transport signatures. As disorder is added to the periodic pinning array, the velocity-force curves develop discrete steps and the oscillating phase is replaced by a strongly fluctuating phase. These effects are similar to shear banding phenomena in complex fluids where different dynamical phases can coexist and couple.

This work was carried out under the auspices of the NNSA of the U.S. DOE at LANL under Contract No. DE-AC52-06NA25396.

[1] H. Rehage and H. Hoffmann, Mol. Phys. **74**, 933 (1991).
[2] J. F. Berret, D. C. Roux, G. Porte, and P. Lindner, Europhys. Lett. **25**, 521 (1994); V. Schmitt, F. Lequeux, A. Pousse, and D. Roux, Langmuir **10**, 955 (1994).
[3] M. M. Britton and P. T. Callaghan, Phys. Rev. Lett. **78**, 4930 (1997).
[4] J.-F. Berret and Y. Séréro, Phys. Rev. Lett. **87**, 048303 (2001).
[5] S. M. Fielding, Soft Matter **3**, 1262 (2007).
[6] S. M. Fielding and P. D. Olmsted, Phys. Rev. Lett. **92**, 084502 (2004).
[7] P. Coussot, J. S. Raynaud, F. Bertrand, P. Moucheront, J. P. Guilbaud, H. T. Huynh, S. Jarny, and D. Lesueur, Phys. Rev. Lett. **88**, 218301 (2002).
[8] D. Lopez, W. K. Kwok, H. Safar, R. J. Olsson, A. M. Petrean, L. Paulius, and G. W. Crabtree, Phys. Rev. Lett. **82**, 1277 (1999).
[9] Y. Paltiel, E. Zeldov, Y. Myasoedov, M. L. Rappaport, G. Jung, S. Bhattacharya, M. J. Higgins, Z. L. Xiao, E. Y. Andrei, P. L. Gammel, and D. J. Bishop, Phys. Rev. Lett. **85**, 3712 (2000).
[10] M. C. Marchetti and D. R. Nelson, Phys. Rev. B **59**, 13624 (1999).
[11] A. Furukawa and Y. Nisikawa, Phys. Rev. B **73**, 064511 (2006).
[12] S. Okuma, S. Morishima, and M. Kamada, Phys. Rev. B **76**, 224521 (2007).
[13] M.-C. Miguel and S. Zapperi, Nature Mater. **2**, 477 (2003).
[14] N. S. Lin, V. R. Misko, and F. M. Peeters, Phys. Rev. Lett. **102**, 197003 (2009).
[15] M. Baert, V. V. Metlushko, R. Jonckheere, V. V. Moshchalkov, and Y. Bruynseraede, Phys. Rev. Lett. **74**, 3269 (1995); V. Metlushko, U. Welp, G. W. Crabtree, R. Osgood, S. D. Bader, L. E. De Long, Z. Zhang, S. R. J. Brueck, B. Ilic, K. Chung, and P. J. Hesketh, Phys. Rev. B **60**, R12585 (1999); A. N. Grigorenko, S. J. Bending, M. J. Van Bael, M. Lange, V. V. Moshchalkov, H. Fangohr, and P. A. J. de Groot, Phys. Rev. Lett. **90**, 237001 (2003); G. Karapetrov, J. Fedor, M. Iavarone, D. Rosenmann, and W. K. Kwok, *ibid.* **95**, 167002 (2005).
[16] J. I. Martín, M. Vélez, J. Nogués, and Ivan K. Schuller, Phys. Rev. Lett. **79**, 1929 (1997); D. J. Morgan and J. B. Ketterson, *ibid.* **80**, 3614 (1998).
[17] M. Kemmler, D. Bothner, K. Ilin, M. Siegel, R. Kleiner, and D. Koelle, Phys. Rev. B **79**, 184509 (2009).
[18] C. Reichhardt, C. J. Olson, and F. Nori, Phys. Rev. Lett. **78**, 2648 (1997).
[19] J. Gutierrez, A. V. Silhanek, J. Van de Vondel, W. Gillijns, and V. V. Moshchalkov, Phys. Rev. B **80**, 140514(R) (2009).
[20] Z. L. Xiao *et al.* (unpublished).
[21] C. Reichhardt and C. J. Olson Reichhardt, Phys. Rev. B **76**, 094512 (2007); **81**, 024510 (2010).